Applied Catalysis B: Environmental 166–167 (2015) 475–484

Contents lists available at ScienceDirect

Applied Catalysis B: Environmental

journal homepage: www.elsevier.com/locate/apcatb

Highly photo-catalytically active hierarchical 3D porous/urchin nanostructured Co_3O_4 coating synthesized by Pulsed Laser Deposition

R. Edla [a], N. Patel [a,b,*], M. Orlandi [a], N. Bazzanella [a], V. Bello [c], C. Maurizio [c], G. Mattei [c], P. Mazzoldi [c], A. Miotello [a]

[a] Dipartimento di Fisica, Università degli Studi di Trento, Via Sommarive 14, I-38123 Povo, Trento, Italy
[b] Department of Physics, University of Mumbai, Vidyanagari, Santacruz (E), Mumbai 400 098, India
[c] Department of Physics and Astronomy, University of Padova, via Marzolo 8, I-35131 Padova, Italy

ARTICLE INFO

Article history:
Received 15 September 2014
Received in revised form
22 November 2014
Accepted 28 November 2014
Available online 4 December 2014

Keywords:
Hierarchical 3D urchin
Co_3O_4
Pulsed Laser Deposition
Dye degradation

ABSTRACT

A porous coating assembled with hierarchical 3D Co_3O_4 urchin-like particles was synthesized by Pulsed Laser Deposition (PLD) and thermal oxidation. Laser ablation of Co—B powder, used as the target material, in oxygen atmosphere formed core–shell particles on the coating surface with mainly a metallic Co core and a mixture of Co, B and O accommodating the shell. The thermal oxidation of these core–shell particles in air at 600 °C induces the morphological transformation to urchin-like particles consisting of nanowires (NWs) (diameter: 30–60 nm and length 1–3 μm) grown radially from the core surface. The extrusion marks on the surface of NWs indicate that the stress induced growth process is caused by difference in the thermal expansion coefficient. XRD, Raman, EXAFS and HRTEM analysis confirmed that the NWs are polycrystalline consisting of pure Co_3O_4 phase. A wet-chemistry hydrothermal procedure was also employed to synthesize nanostructured urchin-like particles which are hollow and the structure is held together by the radially oriented nanorods (diameter: 40–150 nm). During photocatalysis, urchin-like particles synthesized by PLD displayed significantly higher (~5 times) degradation rates when compared to chemical urchins for degradation of methylene blue dye via a photo-Fenton reaction in presence of H_2O_2 and visible light. This is mainly attributed to poor stability of the nanorods in the chemical urchin structure. Features such as high surface area, enhanced stability against agglomeration, polycrystalline nature of the NWs, porous surface and superior adhesion, are responsible for the enhanced photocatalytic activity of Co_3O_4 urchin-like particles assembled in a porous coating synthesized by PLD and thermal oxidation. Reusability tests also demonstrate the robust nature of the catalyst coating.

1. Introduction

Release of various organic pollutants such as textile dyes, phenols, aromatic amines and other carcinogenic materials from many industries is becoming a serious problem. Dyes from textile industries are often organic molecules with complex structures, highly toxic in water, non-biodegradable and a serious concern to the ecosystem [1–3]. Several methods have been commonly employed to neutralize these pollutants, in particular the advanced oxidation process (AOP), involving active species like the hydroxyl-radical ($OH^{\bullet}$) with very high oxidation potential, has been applied with very high efficiency [4]. Radical generation occurs by processes such as direct photolysis of H_2O_2, photo-excitation of TiO_2 and photo-Fenton reaction in presence of H_2O_2 with metal cations [5,6]. However, the first two methods require high intensity UV light while the photo-Fenton reaction proceeds by absorption of visible light hence showing significantly higher efficiency under sunlight. Among metal oxides, the Co_3O_4 based materials are of great interest as a photo-Fenton catalyst due to their low cost, natural abundance, visible light absorption and most importantly the good catalytic activity toward degradation of organic compounds even at neutral pH [6,7].

Development of catalysts with desirable morphology and dimensions is an interesting and challenging task owing to their improved catalytic activity and increasing applications in various fields [8–11]. Hierarchical 3D urchin-like nanostructures are promising for wastewater treatment through heterogeneous photocatalysis because of their high surface area which facilitates

* Corresponding author at: Lab IdEA, Department of Physics, Università degli Studi di Trento, Via Sommarive 14, I-38123 Povo, Trento, Italy. Tel.: +39 0461 28 2012; fax: +39 0461 28 1696.
E-mail addresses: patel@science.unitn.it, nainesh11@gmail.com (N. Patel).

http://dx.doi.org/10.1016/j.apcatb.2014.11.060
0926-3373/

catalysis by providing a larger solid–liquid interface. Hierarchical flower-like $Co_{3-x}Fe_xO_4$ structures [12], hierarchical assemblies of Au and AgI nano-crystals in the Fe_3O_4–SiO_2–Au–Ag–AgI composite particles [13] and three-dimensional semiconductor nano-networks of TiO_2 and ZnO with controlled band gap energies have been highly efficient in degrading the Methylene Blue (MB) dye [14]. Urchin-shaped Fe_3O_4@Bi_2S_3 core–shell hierarchical structures with enhanced photo catalytic efficiency for degradation of Rhodamine B dye (RhB) have been studied recently [15]. Urchin-like iron oxyhydroxide (α-FeOOH) and oxide (α-Fe_2O_3) nanostructures showed very good ability to remove organic pollutants [16], while 3D hierarchical rose-like $Bi_2O_2CO_3$ microspheres have been able to degrade mixture of three dyes with enhanced photo catalytic activity under visible light conditions [17]. Recently, there has been a great interest toward the synthesis of Co_3O_4-based hierarchical 3D nanostructures by chemical methods and their applications in water purification. It was reported that Co_3O_4 hierarchical urchin structures were highly efficient in degrading reactive black dye [18]. The enhanced photocatalytic activity was explained on the basis of features established by obtained nanostructures such as higher crystallinity, increased surface area, morphology derived surface exposed planes and enhanced solid–liquid interaction for adsorption and further catalytic reaction in presence of light. However, all these catalysts are produced primarily in form of powder which has problems related to agglomeration during the reaction and cannot be recovered easily for the reuse, thus contributing to the pollutants. In addition, chemically prepared hierarchical structures do not possess long-term stability. Because of these drawbacks, powders are not suitable for continuous flow water treatment reactors.

Immobilized photocatalysts (IPC) in form of coating with tailored properties supported over a substrate are of great interest in avoiding the above mentioned problems [1,6,7,19,20]. IPC have been synthesized with several methods, including electron-beam deposition (EBD), atomic layer deposition (ALD), plasma-enhanced chemical vapor deposition (PECVD), and sol–gel methods by dip coating [21–25]. In the last decade, Pulsed Laser Deposition (PLD) has gained attention as a viable method of producing high-quality and highly stable coatings [1,7,26]. It is ideally suited for the deposition of a wide variety of materials on various substrates and the laser process allows the production of NPs with desired morphology and particle size as small as 10 nm in the form of nanoparticle-assembled coatings by just tuning the experimental parameters [27].

In this paper, we report for the first time the synthesis of 3D porous/urchin Co_3O_4 nanostructures as IPC on glass substrates by thermal annealing of Cobalt–boride (Co—B) and Co—B—O coatings deposited by PLD in vacuum and in O_2 atmosphere respectively. These structures were systematically characterized and their photocatalytic activity toward degradation of MB dye was studied and compared with that of Co_3O_4NPs-assembled coatings synthesized by PLD and of Co_3O_4 urchin-like structures prepared by hydrothermal synthesis.

2. Experimental

Co—B compound was used as the starting material to synthesize urchin-like structure. Coatings of Co—B were deposited by PLD using KrF excimer laser (Lambda Physik) with an operating wavelength at 248 nm, pulse duration of 25 ns, and repetition rate of 20 Hz. The fluence of laser was always maintained at 3 J/cm^2 for ablation. Details of the PLD deposition apparatus and mechanisms involved in the laser ablation process are presented in our past reports [7,28]. Cold-pressed pellets of Co—B powder (synthesized according to ref [29]) were used as the target material. The PLD chamber was evacuated up to a base pressure of 10^{-6} mbar prior to the deposition. The coatings were deposited on Si and glass by maintaining the target to substrate distance at 4.5 cm. The deposition of Co—B in vacuum or in reactive O_2 atmosphere (pressure of 4.5×10^{-2} mbar, from now on labeled Co—B—O) was carried out at room temperature. For comparison, coatings assembled with Co_3O_4 NPs were also deposited by PLD with the deposition conditions reported in our previous work [6], where these coatings showed the best photocatalytic activity for the degradation of organic dyes [7] and the oxidation of carbon monoxide (CO) [7]. Thermal treatment of all the coatings was carried out in air at three different temperatures (400, 500, 600 °C) for 4 h with a heating rate of 5 °C min^{-1} in order to grow the urchin structure.

Powders of Co_3O_4 urchin-like structures were prepared by an hydrothermal synthesis adapted from literature [30]. Typically, 1 mmol of $Co(NO_3)_2{\cdot}6H_2O$, 3 mmol of NH_4F and 5 mmol of $Co(NH_2)_2$ were dissolved in 35 ml of deionized water and sealed in a custom-built teflon-lined aluminum autoclave with a 50 ml capacity. The reactor was heated at 120 °C for 5 h and allowed to cool down at room temperature. A pink precipitate was then collected by filtering on a sintered glass buchnerfunnel, washed several times with water and isopropanol and dried in air at 70 °C for 45 min. The same procedure was followed to obtain thin films on glass, Si and fused silica substrates by placing them inside the reactor during the process. Thermal treatment of this product was then carried out at 600 °C in air for 4 h with a heating rate of 5 °C min^{-1}.

The surface morphology of all samples was studied by a scanning electron microscope (SEM-FEG, JSM 7001F, JEOL) equipped with energy-dispersive spectroscopy analysis (EDS, INCA PentaFET-x3) to determine the composition of the samples. Transmission Electron Microscopy (TEM) analyses were performed with a field emission FEI TECNAI F20 SuperTwin FEG (S) TEM microscope operating at 200 kV equipped with an EDAX energy-dispersive X-ray spectrometer (EDS). Bright-field TEM (BF-TEM) images, and high-resolution TEM (HR-TEM) images have been recorded. Commercial holey carbon films were used as substrate to prepare samples for TEM analysis. Raman spectra were recorded by using HORIBA JobinYvon Lab RAM Aramis Raman spectrometer with diode pumped solid state laser operating at 634 nm. Structural characterization of all the catalyst powders was performed by X-Ray Diffractometer (XRD) using the Cu Kα radiation (λ = 1.5414 Å) in Bragg-Brentano (θ–2θ) configuration. Extended X-ray Absorption Fine Structure (EXAFS) experiment was performed at Co K-edge at the Italian beam line BM08 of the European Synchrotron Radiation Facility. The monochromator was equipped with a couple of Si (3 1 1) crystals; harmonics rejection was achieved by a couple of Pd-coated mirrors working at an incidence angle of 3.6 mrad. X-ray absorption spectra were recorded from Co—B—O deposited samples at T = 80 K in fluorescence mode using a 12 elements HP Ge detector. The spectrum from a Co_3O_4 powder pellet was recorded in transmission mode as standard reference.

The photocatalytic performance of urchin structures and of Co_3O_4 NPs assembled coatings was evaluated by studying the degradation of the Methylene Blue (MB) dye. 30 ml of 10 ppm MB (Alfa Aesar) dye solution mixed with 1 ml of 0.5 M hydrogen peroxide (H_2O_2) as oxidizing agent were used for degradation by photo-Fenton reaction. The catalyst coatings (glass slide of area 2.5 cm × 7.5 cm) were dipped in the above prepared MB dye solution and kept under stirring at 300 rpm in dark for 30 min to establish adsorption equilibrium between the solution and the catalyst surface. The weight of the catalyst was maintained approximately 1 mg during each course of reaction. A tungsten lamp (225 W) with visible spectrum was used as the light source for the photo-Fenton reaction. 1 ml of MB dye solution was collected after established time intervals during the reaction to study the amount of degradation by measuring the UV–vis absorption spectra and

analyzing the peak at 664 nm which is characteristic of MB dye. Absorption spectra were measured by using a VARIAN Cary 5000 UV–vis–NIR spectrophotometer. All the photocatalysis experiments were performed at room temperature and the pH of solution was maintained neutral. The effect of H_2O_2 concentration on the catalytic behavior of the developed catalyst was also studied. The reusability of the Co_3O_4 catalyst with urchin-like structure was further evaluated by collecting the coating after the degradation reaction, washing it with distilled water and reintroducing it into the dye solution to acquire another run. The sample was recycled for 5 times in a similar manner.

3. Results and discussion

3.1. PLD synthesized porous/urchin-like Co_3O_4 coating

SEM image of as-deposited Co—B—O coating deposited in O_2 atmosphere is presented in Fig. 1a. Spherical particulates with wide size distribution in the range of a few nanometers to 1–3 micrometers were observed on the coating surface. Such morphology can be explained by the phase-explosion process, in which at sufficiently high laser fluence the target material surface reaches a temperature of $\sim 0.9T_c$ (T_c is the thermodynamic critical temperature), causing a very high homogeneous nucleation of vapor bubbles. The target surface then makes a rapid transition from superheated liquid to a matrix of vapor and liquid droplets, which leave the irradiated target surface and get deposited on the substrate [31]. The size and the number density of these particles are related to the laser energy as discussed in earlier papers [7,32]. Bright field TEM image of PLD deposited Co—B—O coating (Fig. 1b) reveals that each particulate acquire a core–shell type structure: the lighter contrast in the shell with respect to the core indicates that the shell is composed by lighter elements. EDS compositional analysis on both core and shell (as indicated in Fig. 1b) confirmed the presence of cobalt and boron atoms along with oxygen on the spherical particulates with atomic ratios of Co:B:O = 1:0.6:0.1 in the core and of Co:B:O = 1:1.5:1.3 in the shell, respectively, suggesting that the core is Co-enriched. Moreover, the uniform contrast in the TEM images all over the core or the shell indicates that these are made by amorphous structures (as confirmed also by XRD analysis).

A similar morphology is observed for Co—B coatings deposited in vacuum except the level of oxygen is very low (Fig. S1 of supporting information). Annealing in air at 600 °C for 4 h induce a morphological transformation in both Co—B and Co—B—O coatings forming urchin-like structures with evolution of nanowires (NWs) from the surface of particulates (Fig. 1c and d, respectively). In addition to urchin, a porous structure is also formed in the coating deposited in the oxygen atmosphere (Co—B—O) (Fig. 1d), while vacuum deposited coatings showed only urchin-like particles (henceforth these coatings will be designated as porous/urchin Co_3O_4 coating and urchin Co_3O_4 coating, respectively). Well-defined urchin-like structures comprised of a spherical core with radially grown NWs on the surface (Fig. 1e) are found on particulates of size above 500 nm while smaller particulate transforms into small NWs (Fig. S2). Surface coverage density of these NWs in urchin-like particles is very high of about $(1.2 \pm 0.2) \times 10^{14}$ NW s/m^2. Smaller diameter of NWs, distributed in narrow range of 30–60 nm, with large length (2–3 μm) provides high aspect ratio of around 100. Extrusion marks on the surface are visible in high magnification image of the NWs suggesting the growth of the NWs is stress induced (Fig. 1f and Fig. S3). Further investigation by HR-TEM indicates that the NWs are polycrystalline with grains of well defined lattice fringes (Fig. 1g). The inter-planar spacing obtained by fast-Fourier transformation (FFT) of the HR-TEM image (Fig. 1h) are in good agreement with that of Co_3O_4 phase (Table S1). EDS compositional analysis performed by focusing the electron beam on NWs reveals that only cobalt and oxygen are present in the NWs with an atomic ratio of O(K)/Co(K) = 1.4 ± 0.4 which is compatible with the Co_3O_4 phase, while boron is only detected on the spherical particles.

Co—B coatings deposited in vacuum were annealed in air at various temperatures (400, 500 and 600 °C) for 4 h to investigate the growth mechanism of the urchin structure. Co—B particles synthesized by laser ablation exhibit a spherical shape with smooth surface (Fig. 2a). After annealing at 400 °C the particles appear to disintegrate to form small nanoparticles (NPs) of size 30–60 nm on the surface (Fig. 2b). Further increase in temperature at 500 °C initiates the evolution of NWs from the surface of the particles (Fig. 2c). However, a complete urchin-like structure with well-developed NWs is obtained only after heat treatment at 600 °C (Fig. 2d).

Raman spectra of these samples are presented in Fig. 3. Except for a minor signal at 192 cm^{-1} and 485 cm^{-1} due to surface oxidation of Co, no specific peak is detected for Co—B coating deposited in vacuum (Fig. 3a). After annealing in oxygen atmosphere at 400 °C and 500 °C the broad peaks at 188, 466, 510, 610, and 664 cm^{-1} corresponding to F_{2g}, E_g, F_{2g}, F_{2g} and A_{1g} modes of vibration, respectively, of Co_3O_4 phase are observed. However, these peaks are blue shifted in comparison to the peaks (192, 485, 525, 626 and 694 cm^{-1}) due to crystallized Co_3O_4 [33,34]. This suggests the partial crystallization of Co_3O_4 where short range order and long range disorders create the surface strain to produce blue shift and broadening in the vibrational peaks. After 600 °C, the peaks are comparatively sharper indicating complete crystallization, but peaks position (190, 478, 518, 616 and 681 cm^{-1}) are still at lower wavenumber than the standard Co_3O_4 vibration modes. This may be attributed to the phonon confinement in the nano-domain created in the NWs of the urchin-like particles [35]. The signal in micro-Raman spectroscopy is basically acquired from the surface or just below the surface via inelastic scattering of the source radiation. To obtain structural information about bulk material, XRD of all the coatings was carried out and reported in Fig. 4. As deposited as well as Co—B coating heat treated at 400 °C display complete amorphous nature. Nevertheless, the pattern of as-deposited Co—B coating showed broad peak centered at roughly 35° assigned to the amorphous state of Co—B alloy. While this peak disappeared for the coating heat-treated at 400 °C suggesting the decomposition of the Co—B phase at this temperature. XRD peaks centered at 19.0°, 31.2°, 36.9°, 39.6°, 44.8°, and 54.5° assigned to the face-centered spinel type cubic structure of Co_3O_4 are observed for the Co—B coating annealed at 600 °C [36,37]. These diffraction peaks correspond to the reflections (1 1 1), (2 0 0), (3 1 1), (2 2 2), (4 0 0), (4 2 2), (5 1 1) and (4 4 0) respectively as acquired from JCPDS data file 009-0418. The calculated crystal size, of 18 ± 5 nm, is smaller than the average diameter (45 nm) of NWs measured by SEM and TEM, indicating that the NWs are composed of several grains with average size of about 18 nm. Very few diffraction peaks are observed for Co—B coating annealed at 500 °C indicating that complete crystallization of 3D urchin-like nanostructures occurs after heat treatment at 600 °C. No diffraction peaks due to metallic cobalt, other cobalt oxides or boron oxides phase are detected in XRD pattern.

The EXAFS analysis of Co—B—O coatings on glass substrate has been performed to enlighten the possible presence of other amorphous Co-oxide phases that would not be detected by diffraction-based techniques. The EXAFS spectrum of Co—B—O coating on glass, annealed at 600 °C for 4 h, is reported in Fig. 5 and compared with the similar spectrum of Co_3O_4 crystalline powder. The full EXAFS analysis indicate that the Co site in the Co—B—O coating is very similar to the average one in Co_3O_4 powder, showing that the most part of Co forms Co_3O_4 crystals and no other relevant phases are present.

In general, the growth of 1D nano-structures like nanorods, nanoneedles etc., involves a catalytic-assisted vapor–liquid–solid

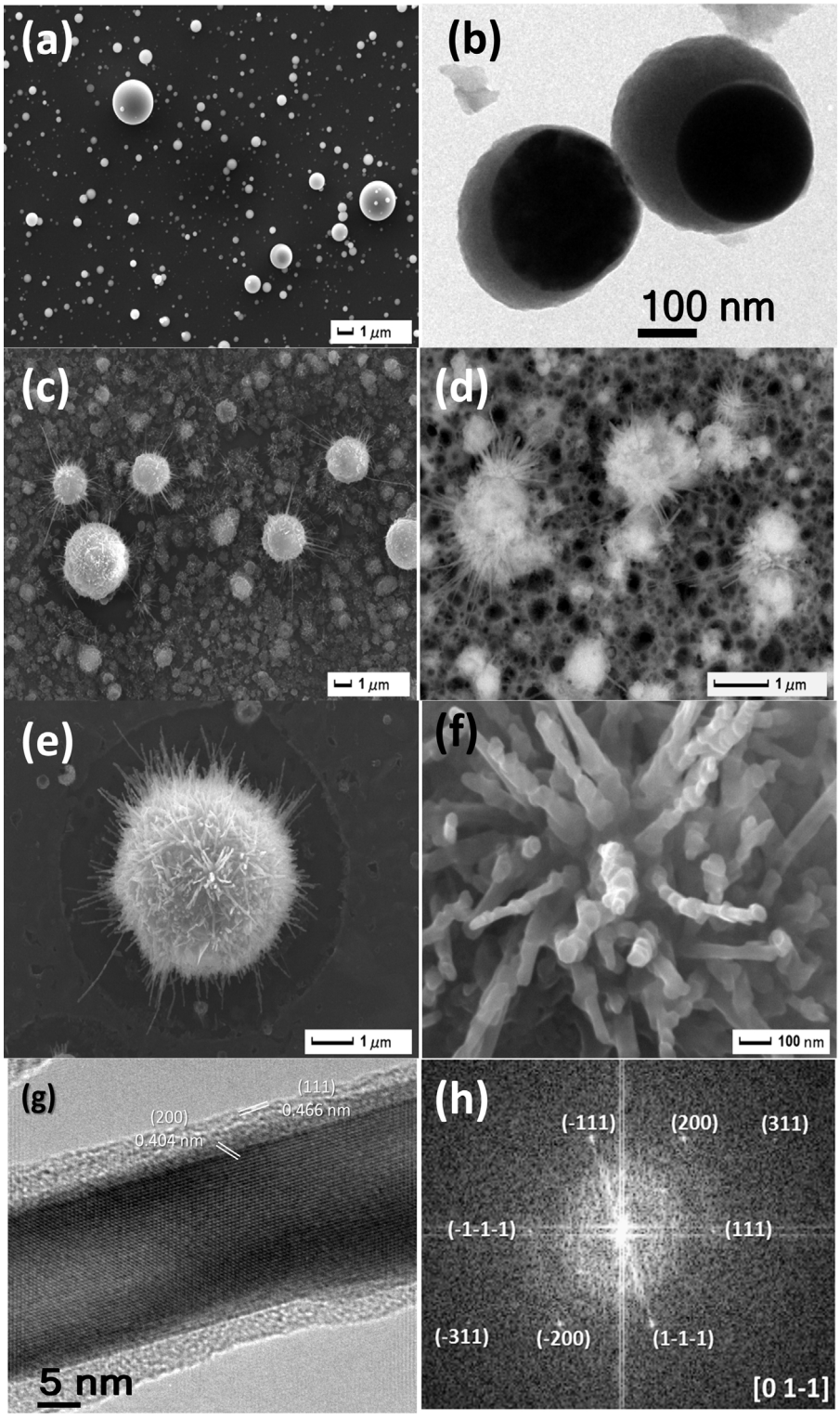

Fig. 1. (a) SEM and (b) bright field TEM image of as-deposited Co—B—O coating prepared by PLD in O_2 atmosphere. SEM image of heat treated, (c) Co—B coating deposited in vacuum and (d) Co—B—O coating deposited in oxygen, at 600 °C for 4 h. SEM image of (e) Urchin-like particle of size ~3 μm and (f) nanowires with extrusion mark over urchin. (g) HRTEM image of NWs showing well arranged lattice fringes and (h) its corresponding fast Fourier transform image.

(VLS) mechanism or vapor–solid (VS) mechanism [38]. For VLS growth, the growth temperature has to be higher than the eutectic temperature of the two elements. In our work, the annealing temperature was well below the eutectic temperature (1100 °C) of cobalt-boron mixture and the melting points of Co (1495 °C), B (2076 °C), and Co_3O_4 (900 °C). Thus VLS and VS mechanisms cannot be responsible for the growth of the urchin nanostructures. Very recently Hsu et al. [39] developed α-Fe_2O_3 urchin-like structures by thermal oxidation of Fe powder in air at similar temperature range where the growth mechanism of nanoflakes is suggested to be selective directional growth via inter-diffusion of oxygen and iron atoms. In order to verify if this type of growth mechanism

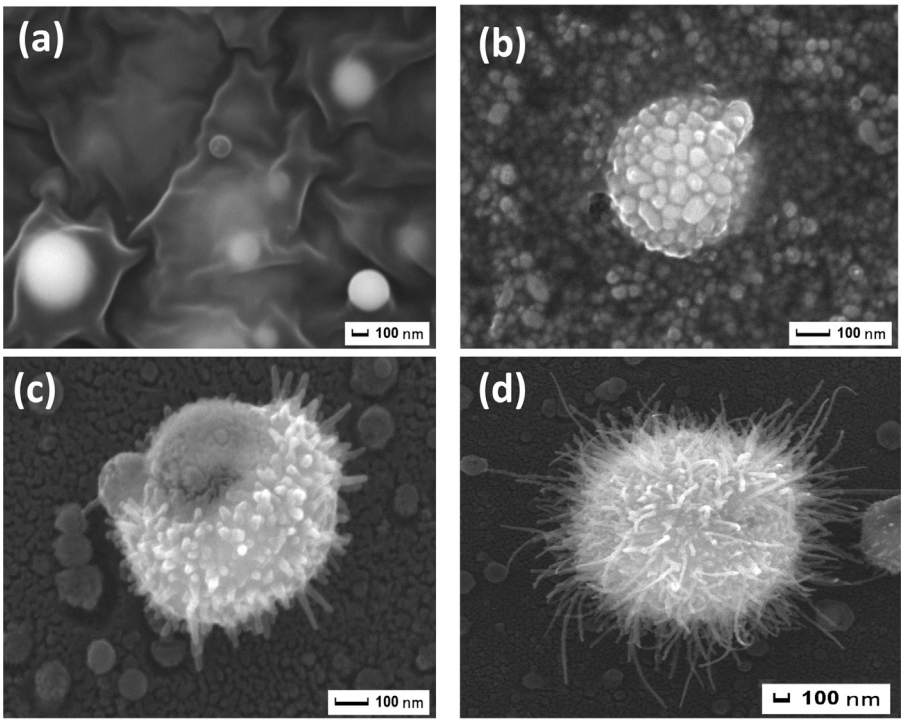

Fig. 2. SEM images of Co—B coating deposited by PLD (a) under vacuum condition and heat treated in air for 4 h at three different temperatures of (b) 400 °C, (c) 500 °C and (d) 600 °C.

also applies to the structures under investigation, Co powder (with particle size of 10 μm) (Fig. S4a) and Co coatings prepared by PLD (Fig. S4b), having similar morphology as Co—B coatings, were annealed in air under similar conditions. No sign of urchin or NWs was observed thus discarding the above mechanism. This shows that boron certainly plays a big role in the urchin formation. On the basis of obtained results a plausible mechanism is proposed here. In as deposited Co—B or Co—B—O coatings, the particulates are of core–shell structure with a cobalt core covered by a shell composed of Co, B and O. During oxidation at 400 °C phase separation might occur in the shell between boron oxide and cobalt oxide forming NPs of the latter. These NPs are under stress condition created by the large difference in the thermal expansion coefficient of boron oxide ($0.5 \times 10^{-6}\,K^{-1}$) and cobalt oxide ($13 \times 10^{-6}\,K^{-1}$). Increasing temperature will further increase the stress level which is released by formation of NWs. The NPs formed in the initial stage act as the nucleating site for the growth of NWs and cobalt is provided from the core for further growth of NWs by outward diffusion. The stress induced growth of NWs is evident from the extrusion marks on the surface of the NWs (Fig. 1f and Fig. S3). Further extensive studies are under way to exactly understand the mechanism of the NWs growth and will be presented in the forthcoming work.

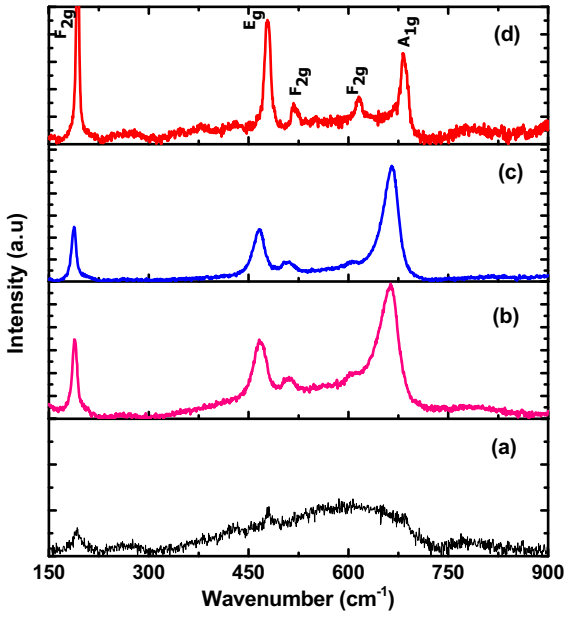

Fig. 3. Raman Spectra of Co—B coating deposited by PLD under (a) vacuum condition and heat treated in air for 4 h at three different temperatures of (b) 400 °C, (c) 500 °C and (d) 600 °C.

3.2. Chemically synthesized urchin-like Co_3O_4 catalyst

Urchin-like nanostructures were synthesized by a hydrothermal method without using any template material (henceforth

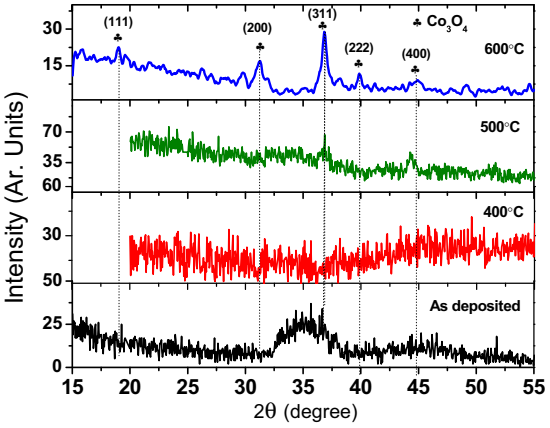

Fig. 4. XRD pattern of Co—B coating deposited by PLD under vacuum condition and heat treated in air for 4 h at three different temperatures of 400 °C, 500 °C and 600 °C.

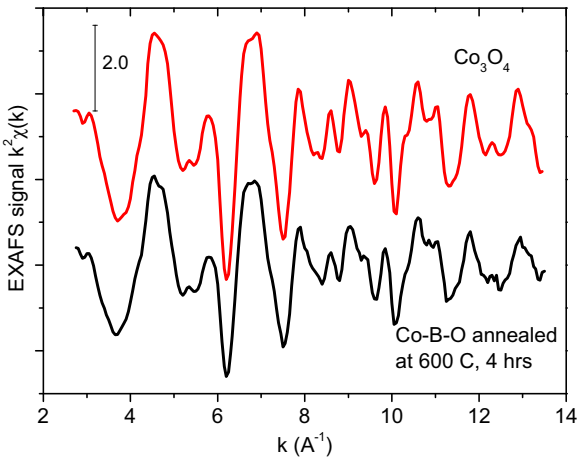

Fig. 5. EXAFS spectrum of Co—B—O coating on glass after annealing in air for 4 h at 600 °C, compared to the very similar spectrum of Co_3O_4 crystalline powder.

designated as chemical urchin). Uniformly distributed urchin-like sphere with size in the range of 8–12 μm were evidently visible in SEM images of as prepared samples (Fig. 6a). High magnification SEM suggests that NWs of length 4–6 μm are tapered with width at bottom around 150–200 nm and of about 50–80 nm at the tip (Fig. 6b). The surface of NWs is highly smooth without any major defects. However, the core in this urchin-like structure is hollow and the complete assembly is thus held by the radially oriented NWs (Fig. S5). Heat treatment at 600 °C in air did not cause any change in the primary urchin-like structure (Fig. S6) but the shape and surface of NWs completely changed. The length of NWs is not affected but the shape has transformed from tapered to rod-like having nearly uniform width from top to bottom. The diameter of these nano-rods varied from 40 to 150 nm as examined through SEM imaging (Fig. 6c). The building blocks of NWs are now composed of irregularly shaped NPs of size 10–30 nm (Fig. 6d). Set of crystalline plane in each NPs are clearly distinguished in HRTEM image (Fig. 6e). The distance between the lattice fringes measured

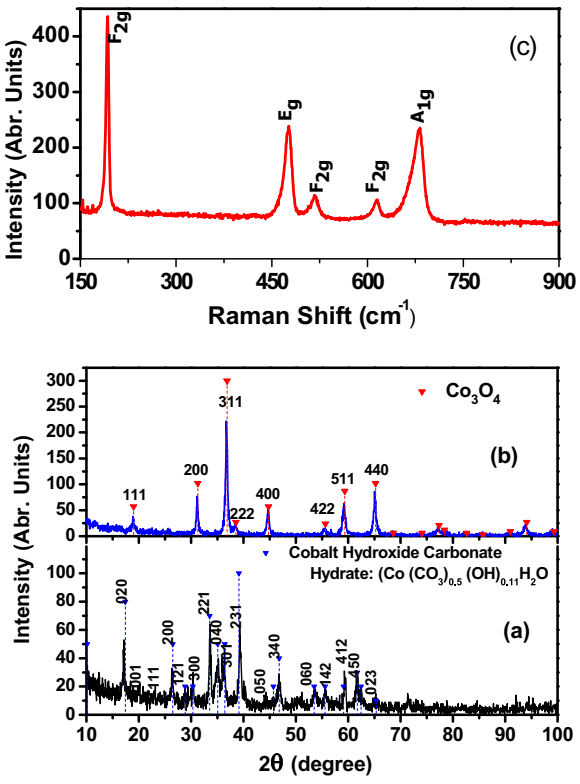

Fig. 7. XRD pattern of (a) as-prepared chemical urchin coating and (b) after heat treatment at 600 °C for 4 h in air. (c) Raman spectra of heat treated chemical urchin Co_3O_4 catalyst at 600 °C for 4 h in air.

by FFT of HRTEM image (Fig. 6f) matches well with the Co_3O_4 phase (Table S2).

XRD pattern (Fig. 7a) of as prepared chemical urchin displayed several diffraction peaks all assigned to the orthorhombic cobalt hydroxide carbonate hydrate ($Co(CO_3)_{0.5}(OH)_{0.11}H_2O$) [30]. After annealing at 600 °C in air total oxidation of urchin occurs as

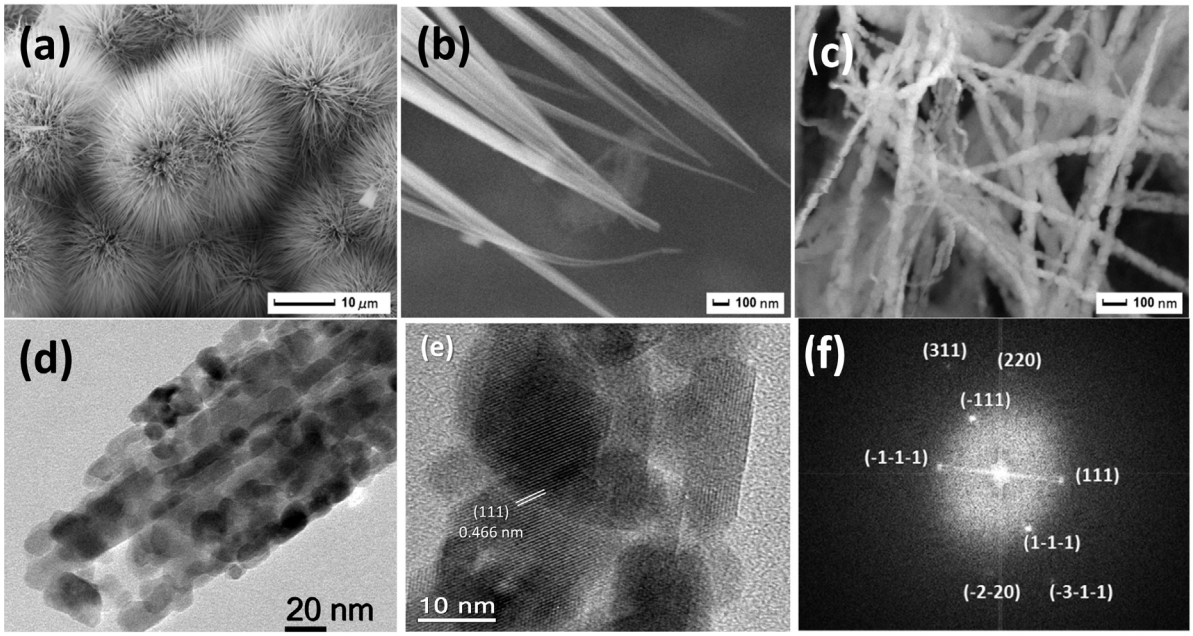

Fig. 6. SEM images of chemically prepared (a) Urchin-like particle by hydrothermal method, (b) tapered NWs in urchin structure, and (c) nanorods obtained after heat treatment of chemical urchin at 600 °C for 4 h in air. (d) Bright field TEM image showing nanorod obtained after heat treatment is composed of nanoparticles, (e) HRTEM of these nanoparticles, and (f) corresponding FFT image.

indicated by XRD which shows only the peaks corresponding to the spinel type cubic structure of Co_3O_4 with Fd3m space group [30] (Fig. 7b). The crystal size of 24 ± 4 nm is in good agreement with the size of NPs in the nano-rod as observed by TEM. The crystallization on the surface was confirmed by Raman spectra showing the vibration modes attributed to the Co_3O_4 phase (Fig. 7c). The mechanism involved in formation of this urchin was well explained by Riu et al. [30] on the basis of experimental evidence. In brief, the process involves formation of microparticles over which one-dimensional NWs grow by dissolution of cores through Ostwald ripening. These NWs disintegrate at high temperatures forming nano-rods assembled with NPs.

3.3. Photocatalytic dye degradation

Photocatalytic activity of the 3D urchin-like nanostructures of Co_3O_4 was studied by degradation of the MB dye through photo-Fenton reaction. In our previous work [6,7], NPs assembled Co_3O_4 coating synthesized by PLD displayed the best degradation-rate of MB dye among the Co_3O_4 coatings produced by various physical and chemical techniques. NPs formed by the laser process show favorable features, such as small average size (18 nm), narrow size distribution ($\sigma = \pm 3$ nm), perfect spherical shape, low degree of agglomeration, and mixed amorphous-nanocrystalline phase, which are mainly responsible for enhanced photocatalytic activity. In order to examine the effectiveness of the present urchin structures obtained by PLD, the photocatalytic activity was compared with Co_3O_4 NPs assembled coating synthesized with PLD. The variation in MB dye concentration vs. irradiation time was measured, through optical absorbance measurements of characteristic peak of the MB dye at 664 nm. The photocatalytic measurement was performed twice by using two different samples synthesized by same parameters in order to establish the reproducibility of the process. The degree of discoloration of the MB dye solution was expressed in the form of degradation ratio $(1 - [A/A_0])$ where A_0 is the absorbance at time $t = 0$ and A is the absorbance at a given reaction time. Adsorption is the major prerequisite condition for any heterogeneous catalytic reaction. Thus all the catalyst coatings were kept in the dye solution in dark for 30 min. Adsorption of dye was 3–5% for urchin and porous/urchin Co_3O_4, while NPs assembled coating was able to adsorb only 1–2% suggesting improved interaction between the catalyst and dye molecules for urchin structures.

Degradation of the MB dye was investigated in presence of only light, with added H_2O_2 and light, and with Co_3O_4 catalyst coating in light. Maximum degradation of 10–15% was measured even after prolonged period of 6–8 h for all three combinations. The dye was completely degraded only when catalyst is exposed to visible light in presence of H_2O_2 oxidant thus indicating that the dye is decolorized by photo-Fenton reaction (further evidence is reported in later section). Fig. 8 represents the rate of degradation of MB dye (10 ppm, 30 ml) in presence of light and H_2O_2 (0.5 M, 1 ml) using Co_3O_4 NPs assembled coating, urchin Co_3O_4 coating or porous/urchin Co_3O_4 coating prepared by PLD as catalyst. In all experiments the weight of the catalyst and the irradiated geometric area were maintained around 1 mg and 2.5 cm × 7.5 cm respectively. The catalytic activity of NPs assembled coating was significantly lower when compared to urchin structures where even after 10 h former was not able to completely degrade MB dye while porous/urchin structures required only 2.5 h to reach 100% degradation. On the other hand, coating with only Co_3O_4 urchin structure produces a colorless solution after 4.5 h. These results show that the porous/urchin structures are more effective than only urchin, but the difference is small indicating that the urchin structure is mainly responsible for the high catalytic activity.

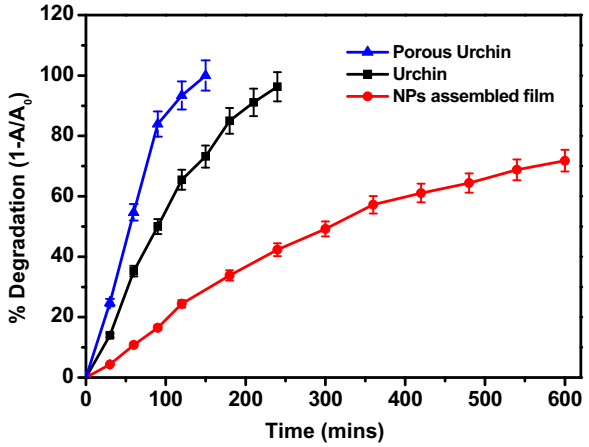

Fig. 8. Time dependent photocatalytic degradation ratio of MB solution (10 ppm, 30 ml) in presence of 1 ml of H_2O_2 (0.5 M) and visible light using different nanostructures (NPs assembled, Urchin and porous/urchin) of Co_3O_4 catalyst coatings prepared by PLD.

To prove this point Co—B coatings deposited in vacuum atmosphere were annealed at different temperatures where the evolution of urchin is monitored and the photocatalyst activity was tested for each step of the growth. Degradation of MB dye solution (10 ppm) using Co—B coatings annealed at 400, 500 and 600 °C, in presence of H_2O_2 (0.5 M, 1 ml) and visible light are presented in Fig. 9. No change in degradation rate was observed for the samples annealed at 400 and 500 °C in comparison to as-deposited Co—B coatings. All three samples degrade only 40% of the dye in 4 h while complete colorless solution is achieved in 4.5 h for urchin Co_3O_4 structure formed after annealing at 600 °C. This result indicates that the crystalline urchin structure is the most effective, because at 500 °C the urchin structure is partially present but not completely crystallized, resulting in activity similar to as deposited coating.

In the past, urchin structures of Co_3O_4 were mainly prepared by hydrothermal synthesis or other wet-chemistry techniques [11,12]. To best of our knowledge, this is the first report on Co_3O_4 urchin structures developed by a physical technique such as PLD. Thus it is necessary to compare the performance of urchin structures prepared by both methods (physical and chemical) for future applications. Chemical Co_3O_4 urchins in form of coating (over glass substrate) and powder were synthesized by hydrothermal method and tested for MB dye (10 ppm) degradation in presence of H_2O_2

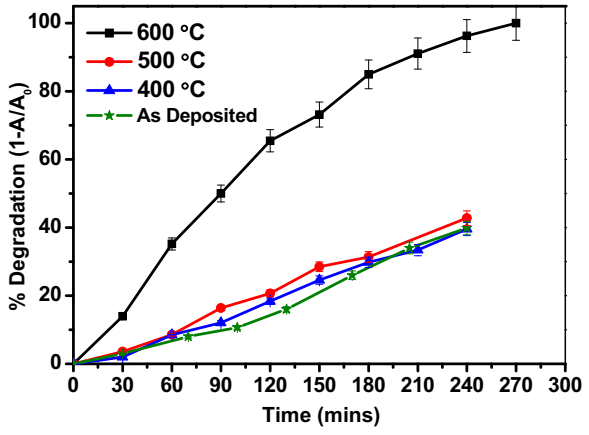

Fig. 9. Time dependent photocatalytic degradation ratio of MB solution (10 ppm, 30 ml) in presence of 1 ml of H_2O_2 (0.5 M) and visible light using Co—B coating deposited by PLD under vacuum condition and heat treated in air for 4 h at three different temperatures of 400 °C, 500 °C and 600 °C.

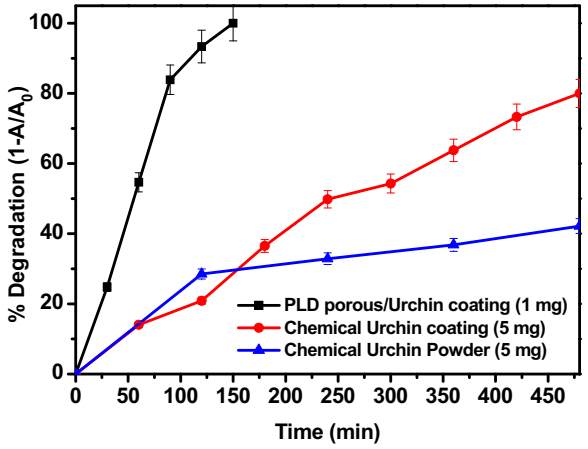

Fig. 10. Time dependent photocatalytic degradation ratio of MB solution (10 ppm, 30 ml) in presence of 1 ml of H_2O_2 (0.5 M) and visible light using Co_3O_4 coatings with porous/urchin structure prepared by PLD and chemical Urchin in form of coating over glass substrate and powder prepared by hydrothermal method.

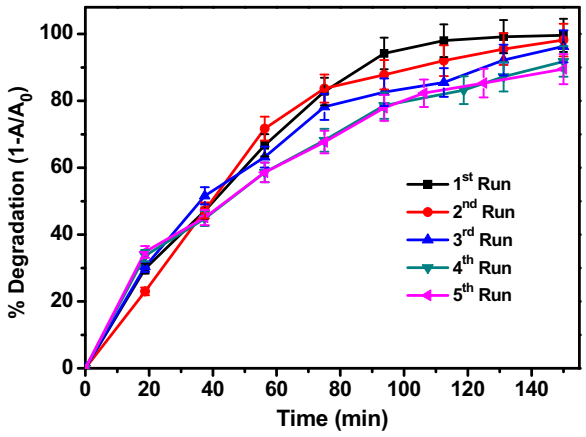

Fig. 12. Recycling behavior of porous/urchin Co_3O_4 coating, prepared by PLD and thermal oxidation in air for 4 h at 600 °C, for MB dye degradation.

(0.5 M, 1 ml) and visible light (Fig. 10). A catalyst amount of 5 mg was required to completely cover the glass slide (2.5 cm × 7.5 cm) and thus a similar amount of Co_3O_4 urchin powder was used for degradation tests. In comparison to the PLD porous/urchin Co_3O_4 coating (1 mg), the chemical Co_3O_4 urchin coating display nearly five times lower degradation rate for MB dye and was able to degrade only 80% in 8 h. However, the chemical urchin in form of coating was better than in powder form which degraded only 57% in 8 h. Agglomeration of urchin like particle in the dye solution during the reaction course may be the primary reason for the reduced catalytic activity for powder chemical urchin. In fact for the first 2 h the degradation rate for coating and powder of chemical Co_3O_4 urchin was similar but the rate falls drastically with time in case of powder. In order to understand the lower catalytic activity, the surface morphology of the chemical Co_3O_4 urchin coating was investigated after dye degradation reaction. SEM image (Fig. 11a) shows that chemical urchin structure completely collapsed and the broken NWs aggregate to form large particles of size 8–10 μm. Since the chemical urchin structure is held by the NWs without core particle, during the constant stirring the friction caused by the aqueous dye solution can disintegrate the urchin. Another important factor is that the NWs are built by the NPs which are loosely bound to each other as observed in TEM images (Fig. 6d). These NPs can be easily separated and cause fragmentation of NWs in the chemical urchin structure, while in the case of PLD prepared Co_3O_4 urchin the structure is well maintained even after the reaction cycle (Fig. 11b). Thus the stability of urchin structure is given by the core from which NWs not only grow but are also strongly held over its surface, keeping the original structure intact even after reaction cycle.

The stability of the PLD prepared Co_3O_4 urchin structure was further investigated by recycling the coating 5 times for degradation of MB dye (10 ppm) in presence of H_2O_2 (0.5 M, 1 ml) and visible light (Fig. 12). After the 5th cycle, 90% degradation was achieved after 2.5 h by PLD synthesized porous/urchin Co_3O_4 coating. This shows that the urchin structure is highly stable on the surface of the coating and strongly attached to the substrate. The minor decrease in the activity is explained in terms of negligible loss of catalyst (0.1 mg) during constant stirring and washing after each run. On the other hand, for NPs assembled Co_3O_4 coating prepared by PLD the degradation decreases to 63% after the 5th cycle. This is attributed mainly to the poor adhesion of the coating leading to the mechanical detachment of the NPs (Fig. S7). Chemical Co_3O_4 urchin coating was not able to operate again for dye degradation due to major loss of catalyst from the substrate, demonstrating poor adhesion.

The enhanced catalytic activity of Co_3O_4 urchins distributed over the porous coating synthesized by PLD and thermal oxidation treatment is mainly attributed to the following features:

1. urchin-like structures with NWs in a narrow size range of 30–60 nm and length of 1–2 μm provide very high surface area for interaction with dye molecules and shorter diffusion path length of photo-generated charge carriers toward the catalyst surface;
2. the core in urchin structures strongly holds the NWs on the surface thus providing high stability against agglomeration of the NWs during the reaction course;

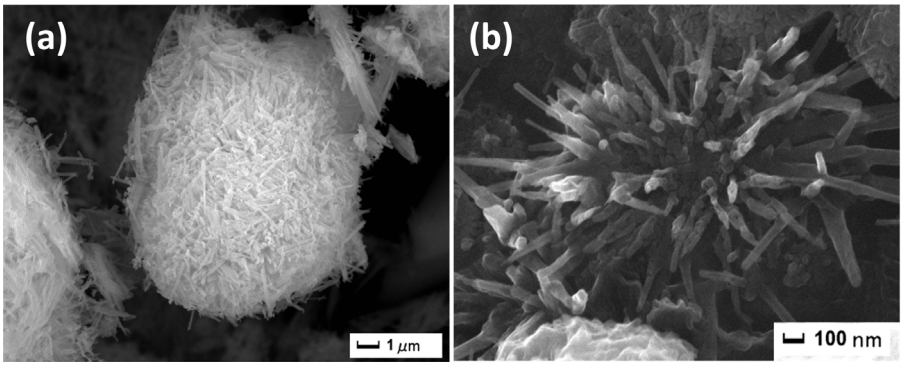

Fig. 11. Morphology obtained by SEM of (a) chemical Co_3O_4 urchin and (b) PLD synthesized Co_3O_4 porous/urchin coatings after MB dye degradation reaction.

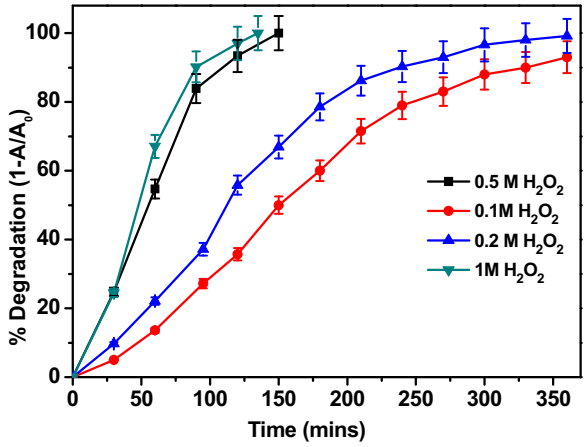

Fig. 13. Photocatalytic degradation efficiency of porous/urchin Co_3O_4 structures with varying the H_2O_2 concentration using 10 ppm of MB dye solution.

3. NWs are polycrystalline in nature possessing a large amount of grain boundaries. These can be considered as linear defects containing atoms with low coordination number as compared to atoms in the ideal bulk crystallites. Thus, these grain boundaries regions are reported to be highly catalytic active sites with basic, acidic or redox functionality [40];
4. porous structures formed on the coating surface not only improve the surface area but also allow the dye molecule to penetrate into the inner surface of the coating to offer higher adsorption of dye molecules;
5. good adhesion of urchin particles prevents aggregation during the reaction course and provides reusability.

In addition, the immobilized nature of coatings permits to easily recover and reuse the catalyst, thus act as ON/OFF switch for the photocatalysis reaction as well as compatibility with continuous flow reactors.

The degradation of MB dye can occur through different mechanisms depending on the route of $OH^{\bullet}$ radical generation: (1) $OH^{\bullet}$ generation by direct photolysis of H_2O_2, this happens only in presence of UV light; (2) $OH^{\bullet}$ generation by photo-excitation of Co_3O_4, this can be ruled out in our case because the standard redox potential of Co^{+3}/Co^{+2} (+1.82 V) is more negative than that of $OH^{\bullet}/OH^{-}$ (+1.99 V); (3) $OH^{\bullet}$ generation by photo-Fenton reaction, where the Co^{+3} and Co^{+2} ions on the surface of the catalyst reacts with H_2O_2 and generates the $OH^{\bullet}$ radicals responsible for dye degradation [5,6]. To prove the photo-Fenton reaction the effect of H_2O_2 concentration on the dye degradation was studied and results are shown in Fig. 13. The degradation efficiency of MB Dye (10 ppm) is enhanced by increasing the H_2O_2 concentration as seen in Fig. 13. In presence of 0.5 M H_2O_2 100% degradation was seen after 2.5 h and after that saturation was attained at 1 M H_2O_2. These results are compatible with a photo-Fenton reaction, where the oxidant concentration is directly proportional to the number of hydroxyl radicals generated and thus increasing the H_2O_2 concentration enhances the degradation rate.

4. Conclusions

Hierarchical 3D Co_3O_4 urchin-like particles have been synthesized in two ways: (1) PLD followed by thermal oxidation (synthesized for the first time), and (2) wet-chemistry hydrothermal procedure.

XRD, Raman, HRTEM and EXAFS analysis shows that urchin-like particles are developed by NWs (diameter: 30–60 nm and length 1–3 μm), of pure Co_3O_4 phase, growing radially from the surface of particulates, produced by laser process, after heat treatment at 600 °C in air. Mechanisms governing PLD urchin are tentatively attributed to stress induced growth process caused by difference in the thermal expansion coefficient in the core–shell structure of the particulates. NPs of cobalt oxide formed during initial stage of phase separation act as nucleating sites for the NWs growth and Co provided by the core sustains growth of NWs by outward diffusion-oxidation process. In case of wet-chemistry hydrothermal synthesis, the urchin-like particles are hollow and the structure is held together by the radially oriented nanorods (40–150 nm, made by assembled Co_3O_4 NPs of size 10–30 nm). The efficiency of these urchin-like nanostructures in photocatalysis was examined and compared by degradation of methylene blue dye via a photo-Fenton reaction in presence of H_2O_2 and visible light. PLD nanostructures displayed significantly higher (~5 times) degradation rates when compared to chemically synthesized urchins: the former requires only 2.5 h for complete dye degradation as compared to the latter degrading 80% of dye in 8 h. High surface area, enhanced stability against agglomeration, polycrystalline nature of the NWs, porous surface, and superior adhesion, are responsible for the enhanced photocatalytic activity of Co_3O_4 PLD urchins. Reusability tests also proved the robust nature of the PLD urchins.

Acknowledgements

We thank C. Cestari for technical support in realizing the apparatus for wet-chemistry hydrothermal process. The research activity is partially supported by the Provincia Autonoma di Trento project ENAM in cooperation with Istituto PCB of CNR (Italy). The EXAFS experiment used the Italian beam time of BM08 at ESRF. We acknowledge Francesco D'Acapito for providing assistance during measurements.

Appendix A. Supplementary data

Supplementary data associated with this article can be found, in the online version, at http://dx.doi.org/10.1016/j.apcatb.2014.11.060.

References

[1] T. Warang, N. Patel, R. Fernandes, N. Bazzanella, A. Miotello, Appl. Catal B: Environ. 132–133 (2013) 204–211.
[2] U.I. Gaya, A.H. Abdullah, J. Photochem. Photobiol. C: Photochem. Rev. 9 (2008) 1–12.
[3] S. Ahmed, M.G. Rasul, W.N. Martens, R. Brown, M.A. Hashib, Desalination 261 (2010) 3–18.
[4] R. Andreozzi, V. Caprio, A. Insola, R. Marotta, Catal. Today 53 (1999) 51–59.
[5] R. Bauer, G. Waldner, H. Fallmann, S. Hager, M. Klare, T. Krutzler, S. Malato, P. Maletzky, Catal. Today 53 (1999) 131–144.
[6] T. Warang, N. Patel, A. Santini, N. Bazzanella, A. Kale, A. Miotello, Appl. Catal. A: Gen. 423–424 (2012) 21–27.
[7] R. Edla, N. Patel, Z. El Koura, R. Fernandes, N. Bazzanella, A. Miotello, Appl. Surf. Sci. 302 (2014) 105–108.
[8] Z. Ren, Y. Guo, C.-H. Liu, P.-X. Gao, Front. Chem. 1 (2013) 1–22.
[9] P. Sun, Z. Zhu, P. Zhao, X. Liang, Y. Sun, F. Liu, G. Lu, CrystEngComm 14 (2012) 8335–8337.
[10] M.E.G. Lyons, M.P. Brandon, J. Electroanal. Chem. 641 (2010) 119–130.
[11] X. Rui, H. Tan, D. Sim, W. Liu, C. Xu, H.H. Hng, R. Yazami, T.M. Lim, Q. Yan, J. Power Sources 222 (2013) 97–102.
[12] J. Hao, W. Yang, Z. Zhang, S. Pan, B. Lu, X. Ke, B. Zhang, J. Tang, Nanoscale 5 (2013) 3078–3082.
[13] Y. Hu, Z. Li, Y. Sun, Catal. Today 225 (2014) 177–184.
[14] H. Ceylan, C. Ozgit-Akgun, T.S. Erkal, I. Donmez, R. Garifullin, A.B. Tekinay, H. Usta, N. Biyikli, M.O. Guler, Sci. Rep. 3 (2013) 1–7.
[15] S. Luo, F. Chai, L. Zhang, C. Wang, L. Li, X. Liu, Z. Su, J. Mater. Chem. 22 (2012) 4832–4836.
[16] J. Fei, Y. Cui, J. Zhao, L. Gao, Y. Yang, J. Li, J. Mater. Chem. 21 (2011) 11742–11746.
[17] P. Madhusudan, J. Zhang, B. Cheng, G. Liu, CrystEngComm 15 (2013) 231–240.
[18] H. Li, G.T. Fei, M. Fang, P. Cui, X. Guo, P. Yan, L.D. Zhang, Appl. Surf. Sci. 257 (2011) 6527–6530.
[19] H.W.P. Carvalho, A.P.L. Batista, P. Hammer, T.C. Ramalho, J. Hazard. Mater. 184 (2010) 273–280.

[20] C.M. Ling, A.R. Mohamed, S. Bhatia, Chemosphere 57 (2004) 547–554.
[21] F. Švegl, B. Orel, I. Grabec-Švegl, V. Kaučič, Electrochim. Acta 45 (2000) 4359–4371.
[22] M.E. Donders, H.C.M. Knoops, M.C.M. van, W.M.M. Kessels, P.H.L. Notten, J. Electrochem. Soc. 158 (2011) G92–G96.
[23] J. Wöllenstein, M. Burgmair, G. Plescher, T. Sulima, J. Hildenbrand, H. Böttner, I. Eisele, Sens. Actuators B: Chem. 93 (2003) 442–448.
[24] V. Balouria, S. Samanta, A. Singh, A.K. Debnath, A. Mahajan, R.K. Bedi, D.K. Aswal, S.K. Gupta, Sens. Actuators B: Chem. 176 (2013) 38–45.
[25] C. Guyon, A. Barkallah, F. Rousseau, K. Giffard, D. Morvan, M. Tatoulian, Surf. Coat. Technol. 206 (2011) 1673–1679.
[26] N. Patel, R. Fernandes, G. Guella, A. Miotello, Appl. Catal. B: Environ. 95 (2010) 137–143.
[27] S.C. Singh, H. Zeng, Sci. Adv. Mater. 4 (2012) 368–390.
[28] A. Miotello, N. Patel, Appl. Surf. Sci. 278 (2013) 19–25.
[29] N. Patel, A. Miotello, V. Bello, Appl. Catal. B: Environ. 103 (2011) 31–38.
[30] X.A. Rui, H. Tan, D. Sim, W. Liu, C. Xu, H.H. Hng, R. Yazami, T.M. Lim, Q. Yan, J. Power Sources 222 (2013) 97–102.
[31] A. Miotello, R. Kelly, Appl. Phys. A. 69 (1999) S67–S73.
[32] N. Patel, G. Guella, A. Kale, A. Miotello, B. Patton, C. Zanchetta, L. Mirenghi, P. Rotolo, Appl. Catal. A: Gen. 323 (2007) 18–24.
[33] I. Lorite, J.J. Romero, J.F. Fernández, J. Raman Spectrosc. 43 (2012) 1443–1448.
[34] V.G. Hadjiev, M.N. Iliev, I.V. Vergilov, J. Phys. C: Solid State Phys. 21 (1988) L199.
[35] C.Y. Xu, P.X. Zhang, L. Yan, J. Raman Spectrosc. 32 (2001) 862–865.
[36] Z.-W. Fu, Y. Wang, Y. Zhang, Q.-Z. Qin, Solid State Ionics 170 (2004) 105–109.
[37] D. Liu, X. Wang, X. Wang, W. Tian, Y. Bando, D. Golberg, Sci. Rep. 3 (2013).
[38] H.J. Fan, P. Werner, M. Zacharias, Semicond. Nanowires 2 (2006) 700–717.
[39] H.-C. Yu, L.-C. Hsu, T.-H. Chang, Y.-Y. Li, Dalton Trans. 41 (2012) 723–726.
[40] J. Tyczkowski, R. Kapica, J. Łojewska, Thin Solid Films 515 (2007) 6590–6595.